Cerebral Cortex Advance Access published April 21, 2015

OXFORD

Cerebral Cortex, 2015, 1–17

doi: 10.1093/cercor/bhv073
Original Article

ORIGINAL ARTICLE

Co-Activation-Based Parcellation of the Lateral Prefrontal Cortex Delineates the Inferior Frontal Junction Area

Paul S. Muhle-Karbe[1], Jan Derrfuss[2], Margaret T. Lynn[1], Franz X. Neubert[3], Peter T. Fox[4], Marcel Brass[1], and Simon B. Eickhoff[5,6]

[1]Department of Experimental Psychology, Ghent University, Ghent, Belgium, [2]School of Psychology, University of Nottingham, Nottingham, UK, [3]Department of Experimental Psychology, University of Oxford, Oxford, UK, [4]Research Imaging Institute, University of Texas Health Science Center San Antonio, San Antonio, TX, USA, [5]Institute of Clinical Neuroscience and Medical Psychology, Heinrich-Heine University Düsseldorf, Düsseldorf, Germany, and [6]Brain Network Modeling Group, Institute of Neuroscience and Medicine (INM-1) Research Center Jülich, Jülich, Germany

Address correspondence to Paul S. Muhle-Karbe, Department of Experimental Psychology, Ghent University, Henri Dunantlaan 2, B-9000 Ghent, Belgium. Email: paulsimon.muhlekarbe@ugent.be

Abstract

The inferior frontal junction (IFJ) area, a small region in the posterior lateral prefrontal cortex (LPFC), has received increasing interest in recent years due to its central involvement in the control of action, attention, and memory. Yet, both its function and anatomy remain controversial. Here, we employed a meta-analytic parcellation of the left LPFC to show that the IFJ can be isolated based on its specific functional connections. A seed region, oriented along the left inferior frontal sulcus (IFS), was subdivided via cluster analyses of voxel-wise whole-brain co-activation patterns. The ensuing clusters were characterized by their unique connections, the functional profiles of associated experiments, and an independent topic mapping approach. A cluster at the posterior end of the IFS matched previous descriptions of the IFJ in location and extent and could be distinguished from a more caudal cluster involved in motor control, a more ventral cluster involved in linguistic processing, and 3 more rostral clusters involved in other aspects of cognitive control. Overall, our findings highlight that the IFJ constitutes a core functional unit within the frontal lobe and delineate its borders. Implications for the IFJ's role in human cognition and the organizational principles of the frontal lobe are discussed.

Key words: cognitive control, inferior frontal junction, meta-analysis, prefrontal cortex

Introduction

The inferior frontal junction (IFJ) is located in the posterior lateral prefrontal cortex (LPFC) at the intersection of the inferior precentral and the inferior frontal sulci. Initially, this area was identified as exhibiting activation associated with cognitive control in the Stroop task and during task-switching (Brass and von Cramon 2002, 2004a, 2004b; Derrfuss et al. 2004, 2005; Neumann et al. 2005). Based on these findings, Brass, Derrfuss, et al. (2005) proposed that the IFJ constitutes "a separable area" within the LPFC that "plays a pivotal role in cognitive control" (p. 314). In particular, it was assumed that this area is involved in the activation of currently relevant task representations. More recent studies indicate that the function of the IFJ is even more general than originally assumed given its involvement in a number of additional

capacities, among them the control of selective visual attention (Asplund et al. 2010; Baldauf and Desimone 2014), dual-tasking (Dux et al. 2006, 2009; Tombu et al. 2011), the implementation of novel instructions (Ruge and Wolfensteller 2010; Hartstra et al. 2011), the detection of behaviorally salient events (Chikazoe et al. 2009; Verbruggen et al. 2010; Levy and Wagner 2011), and the encoding of stimuli into short-term memory (Zanto et al. 2010, 2011; Sneve et al. 2013).

While these findings clearly indicate that the IFJ is involved in very basic cognitive control processes, they also emphasize that its precise role in human cognition remains elusive. One particular reason for this ambiguity is the location of this area at the intersection of seemingly disparate functional domains (Fig. 1). Ventrally it borders Broca's area (Brodmann area [BA] 44), which is implicated in linguistic processing (Hagoort 2005; Friederici and Gierhan 2013), caudally the precentral gyrus (BA 6), which is associated with motor control and action recognition (Wise 1985; Rizzolatti et al. 2002; Davare et al. 2006), dorsally the frontal eye field (FEF; BA 8), which is involved in spatial attention and the control of saccadic eye movements (Paus 1996; Corbetta et al. 1998; Corbetta and Shulman 2002), and rostrally the mid-dorsolateral prefrontal cortex (mid-DLPFC; BA 9/46v), which is also implicated in cognitive control (MacDonald et al. 2000; Petrides 2000; Curtis and D'Esposito 2003). The close proximity of the IFJ to these different domains, along with the fact that empirically derived activations frequently spread across multiple regions, has hindered a more precise characterization of its function.

Functional neuroimaging studies indicate that some of the aforementioned domains might be distinguishable within the LPFC. For instance, cognitive control-related foci in the IFJ have been spatially separated from linguistic functions of Broca's area (Fedorenko et al. 2012) as well as from oculomotor functions of the inferior FEF (Derrfuss et al. 2012). However, the transition from the IFJ to the mid-DLPFC is still poorly understood. Some evidence points toward an organization of the LPFC along its rostrocaudal axis, with more rostral regions being involved in increasingly abstract control functions (Koechlin et al. 2003; Badre and D'Esposito 2007, 2009; Koechlin and Summerfield 2007; Nee and Brown 2012; Nee et al. 2013). From this perspective, the mid-DLPFC might impose higher-order constraints upon more concrete computations in the IFJ. Yet, other findings emphasize the broad domain generality of LPFC regions across diverse types of cognitive demand, questioning the idea of regionally specialized control functions (e.g., Woolgar et al. 2011; Reynolds et al. 2012; Fedorenko et al. 2013; Crittenden and Duncan 2014). Overall, task-based neuroimaging might be limited in revealing the exact subdivisions of the LPFC. For the most part, it is used as a confirmatory method, that is, for the mapping of predefined functions onto neural structures. As such, it presupposes knowledge about the relevant functional properties and it is controversial to what extent current psychological concepts map onto the human brain [see Poldrack (2006)].

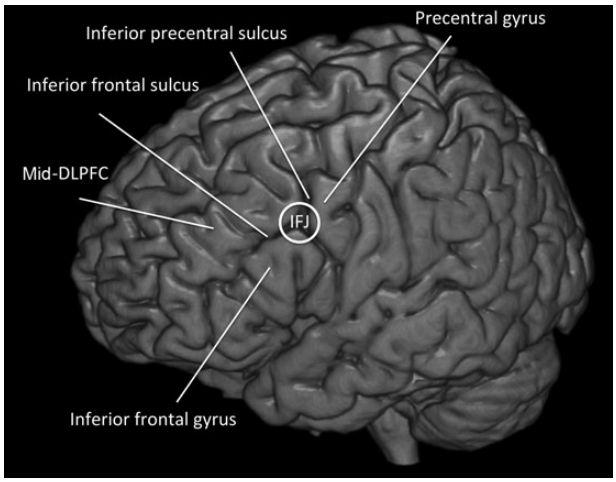

Figure 1. Illustration of the anatomical locations of the IFJ and adjacent areas within the LPFC.

Data-driven parcellation techniques provide a complementary approach toward the delineation of cortical modules. This methodology is motivated by the notion that the function of a brain region is ultimately constrained by its connections with other areas (Passingham et al. 2002), which implies that functional units should be distinguishable based on the dissimilarity of their connections. Various parcellation techniques have been employed in the literature, reflecting the multiplicity of concepts that are used to quantify connections between brain regions such as diffusion-weighted tractography (e.g., Johansen-Berg et al. 2004), resting-state functional connectivity (RSFC; Kelly et al. 2010; Power et al. 2011; Yeo et al. 2011; Kahnt et al. 2012; Gordon et al. 2014), task-based co-activation (Laird et al. 2013), or combinations of those modalities (Mars et al. 2011; Neubert et al. 2013; Sallet et al. 2013). The unifying principle of these methods is to initially divide a volume-of-interest (VOI) into subregions, based on a particular algorithm to quantify connections, which is typically followed by a post hoc characterization of the ensuing divisions (e.g., by comparing the location, extent, and connections of each subregion with existing data from the literature). Thus, parcellation studies cannot only provide anatomical landmarks, but also generate new functional hypotheses that can subsequently be tested in mapping studies. Accordingly, task-based neuroimaging and connection-based parcellation approaches follow different inferential principles and should thus be considered as mutually informative.

Recent parcellation studies have also examined the organization of the LPFC (e.g., Amunts et al. 2010; Kelly et al. 2010; Power et al. 2011; Yeo et al. 2011; Cieslik et al. 2012; Sallet et al. 2013; Neubert et al. 2014), yielding partly inconclusive results. Multiple RSFC studies have examined modularization at the level of the entire neocortex via clustering (Yeo et al. 2011), community detection (Power et al. 2011), or independent-component analyses (Smith et al. 2009). These studies consistently point toward a rather large and homogenous region spanning the inferior frontal sulcus (IFS) as part of a distributed fronto-parietal network. Recent studies have utilized more constrained seed regions (Neubert et al. 2014) or employed more detailed analysis approaches that permit the identification of within-network boundaries (Gordon et al. 2014; Wig et al. 2014). These investigations indicate that a more fine-grained organization may exist within the IFS. For instance, Neubert et al. (2014) employed a comprehensive parcellation of the ventrolateral frontal cortex on the basis of diffusion-weighted tractography and RSFC. They identified a subregion that resembled previous descriptions of the IFJ in extent and location (e.g., Derrfuss et al. 2005, 2009), indicating that it may indeed constitute a separable cortical entity with unique anatomical and functional connections. However, another study that parcellated the left inferior frontal cortex, on the basis of its receptorarchitecture, identified 2 distinct subregions at the junction of the inferior frontal and the inferior precentral sulci (Amunts et al. 2010), suggesting that the IFJ may itself comprise multiple divisions. These divergent findings

illustrate both the unclear functional anatomical basis of the IFJ and the challenge of obtaining stable parcellation schemes that generalize across different methods and modalities. Furthermore, the functional relevance of the aforementioned studies for human cognition remains an open issue, as they were based either solely on structural or architechtonical criteria, or on functional connectivity during the task-free "resting state." Although the latter may reflect the statistical history of regional co-activation (Donsenbach et al. 2007), its precise correspondence to task-based cognitive states remains challenging to establish.

In the present study, we therefore wished to shed new light on the functional neuroanatomical basis of the IFJ. To this end, we employed a co-activation-based parcellation (CBP) of the left IFS and the adjacent parts of the precentral, inferior frontal, and middle frontal gyri (MFG) with the goal of isolating the IFJ. CBP is a relatively new meta-analytic technique that accesses the foci of several thousand experiments that are documented in the BrainMap database and establishes neural modularization via cluster analyses of voxel-wise co-activation patterns [see Eickhoff et al. (2011), Laird et al. (2013), and Fox et al. (2014)]. Thus, in contrast to most other parcellation methods (e.g., DTI, RSFC, cytoarchitecture, and receptorarchitecture), CBP relies on functional brain activation during task performance. Furthermore, the systematic taxonomic labeling of studies in the BrainMap database permits a post hoc functional characterization of the ensuing clusters. Thus, CBP cannot only reveal anatomical entities, but also characterize the differential task sets that reliably engage these units. As such, it provides a powerful tool for revealing functional organization in a data-driven manner. Here, we used CBP to examine if it is possible to delineate one or multiple IFJ regions on the basis of specific task-dependent co-activation patterns, and to reveal the borders to adjacent functional domains with a particular focus on the transition from the IFJ to the more rostral mid-DLPFC.

Materials and Methods

Definition of the VOI

The seed VOI was generated on the basis neuroanatomical criteria using the Mango software ("multi-image analysis GUI"; http://ric.uthscsa.edu/mango) and the MNI152 template in 2-mm resolution. The VOI was oriented along the left IFS (L IFS; Y-coordinates between −6 and +36) and designed to cover a sufficient cortical surface to identify one or multiple IFJ regions, and to delineate its borders to neighboring areas in all directions. As a consequence, it extended deep into the cortex (X-coordinates between −26 and −60), and encompassed parts of the adjacent inferior frontal, middle frontal, and precentral gyri. The insular cortex/frontal operculum was omitted from the seed region. Altogether, the resulting volume included parts of BAs 6, 9, 44, 45, and 46 with a total size of 3815 voxels (voxel size = 4 × 4 × 4 mm; see Fig. 1 for an illustration). Note that our aim was not to provide a comprehensive large-scale parcellation of the entire LPFC [see, e.g., Power et al. (2011), Yeo et al. (2011), Sallet et al. (2013), and Neubert et al. (2014)], but instead to test if one or multiple IFJ regions can be identified as exhibiting unique functional connections, and to characterize the borders with adjacent modules. Moreover, our focus in this study was on the left hemisphere because studies from our laboratories have found activation of the left IFJ more frequently (e.g., Brass and von Cramon 2004a, 2004b; Derfuss et al. 2012; Muhle-Karbe, De Baene, et al. 2014), and this permitted us to reveal borders of the IFJ(s) to the language domain (see Discussion; Fig. 2).

Meta-Analytic Co-Activation Modeling

In the first analysis step, a whole-brain co-activation profile was generated for each voxel within the VOI. These profiles should display the co-activation probability of a given seed voxel with every other voxel in the target brain volume. To this end, we used the BrainMap database to identify studies that reported foci at the respective locations (www.brainmap.org; Fox and Lancaster 2002; Laird et al. 2005; Fox et al. 2014). BrainMap contains the archived foci of several thousand published neuroimaging experiments. These studies are furthermore coded with regard to formal characteristics such as sample sizes, population, or the employed behavioral domain (BD) and paradigm class (PC) in a standardized taxonomy. For the given purposes, studies were only included in the analysis if the samples consisted of healthy adults (i.e., studies with pathological populations or children were excluded) and if they were coded as "normal mapping studies" (i.e., intervention studies and group comparisons were excluded). Moreover, we restricted the analysis to peaks reflecting task-based activations, and discarded deactivations from the analysis. This resulted in approximately 7500 eligible experiments. Moreover, given that the number of studies that report foci at a particular voxel is typically too small and variable for reliable meta-analyses [see Cieslik et al. (2012), Bzdok et al. (2013), and Clos et al. (2013)], we employed spatial filtering across neighboring voxels. That is, in order to obtain a sufficient number of experiments for each seed voxel, we pooled across experiments that reported the most proximate foci, as measured by Euclidian distances. Importantly, the extent of this spatial filter was systematically varied, including the closest 20–200 experiments in

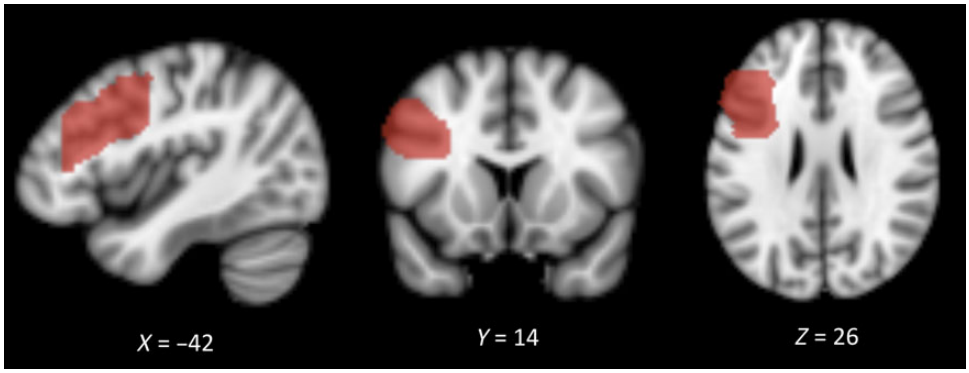

Figure 2. Illustration of the seed VOI in the sagittal, coronal, and transversal plane.

steps of 5, resulting in 37 different filter sizes. This initial range was selected to exclude filter sizes that are unlikely to be useful for the given purposes. As such, meta-analyses with very few experiments do not produce reliable co-activation patterns. Conversely, filtering over extremely large numbers of experiments ultimately prevents the detection of local differences.

For each voxel and filter size, an activation likelihood estimation (ALE) meta-analysis was performed across the respective set of experiments, to reveal concordance of whole-brain co-activation. The general principle of the ALE method is to treat the foci of single studies as 3D Gaussian probability density distributions rather than as single coordinates, reflecting the spatial uncertainty of neuroimaging data (Turkeltaub et al. 2002). For each contributing experiment, a modeled activation map is computed by combining the Gaussian distributions of all reported foci. The voxel-wise union of modeled activation maps across all selected experiments then yields an ALE score for each voxel of the brain (Turkeltaub et al. 2012). This score reflects the probability of the target voxel being co-activated with the seed voxel. Notably, ALE scores were not thresholded at this point to retain all quantitative information about the whole-brain patterns of co-activation. As a consequence of the selected filter range, this procedure resulted in 37 $N_S \times N_T$ co-activation matrices, where N_S refers to the number of seed voxels in the VOI (3815 voxels) and N_T refers to the number of target voxels in the reference brain volume at 4 × 4 × 4 mm (~30 000 voxels).

K-Means Cluster Analyses

Having generated co-activation profiles for all seed voxels, the subsequent series of analyses aimed at parcellating the VOI into clusters of voxels based on the similarity of their co-activation profiles. To this end, the *K*-means cluster method was used. *K*-means is a nonhierarchical cluster method that uses an iterative algorithm to divide the seed region into a pre-selected number of *K* non-overlapping clusters (Hartigan and Wong 1979), with the aim of minimizing the variance within clusters and maximizing the variance between clusters. Initially, the cluster centroids are placed at random and seed voxels are then assigned to the clusters difference from the centroid. One minus the correlation between the co-activation profiles of 2 voxels was used as distance metric. The advantage of the *K*-means cluster method, in comparison with hierarchical cluster methods, is its reduced sensitivity to local features. In hierarchical cluster methods, the assignment of voxels to clusters cannot change anymore after their first assignment, which may result in locally optimal but globally suboptimal solutions. We performed *K*-means clustering for 8 different cluster numbers *K*, ranging from 2 up to 9 clusters. For each cluster number *K*, we performed 10 iterations of the clustering with different randomly selected locations of the initial cluster centroids. Moreover, to further minimize the effects of potential local minima, each iteration was replicated 250 times and only the most stable solution (i.e., the solution with the lowest total sum of distances) was retained (see http://mathworks.com/help/stats/k-means-clustering.html#brah7f_-1 for details). Thus, altogether, the *K*-means cluster analysis yielded a total of 2960 cluster solutions (i.e., 10 iterations × 8 numbers of clusters × 37 spatial filters).

Selection of the Optimal Filter Range

Prior to determining the optimal number of clusters, we reduced the overall range of spatial filters to select a set of filter sizes that produced the most stable cluster solutions [see Clos et al. (2013) and Eickhoff et al. (2014)]. Specifically, we assessed the consistency of the cluster assignments for individual voxels across different filter sizes and selected the range with the lowest number of deviants (i.e., voxels that were assigned differently, when compared with the cluster that a voxel was most frequently assigned to across all filter sizes). In other words, we sought to select filter sizes that produced solutions most similar to the consensus solution. As illustrated in Figure 3, the proportion of deviant voxels was smallest with an intermediate filter size and increased with very small filter sizes, but also with very large filter sizes. The number of deviant voxels was z-normalized within each cluster solution *K*, and the borders of the optimal filter range (45–190 experiments) were defined on the basis of the increase of z-scores before and after the values (i.e., filter sizes with a z-score greater than 0 were removed; Fig. 3*B*). Accordingly, all subsequent analyses were restricted to this filter range. Note, however, that this selection might depend to some degree on the initial filter range specified above. Although this range is empirically plausible (see considerations above), the exact determination of its borders is ultimately arbitrary. Previous CBP studies have often observed a central tendency in the selection of the optimal filer range (i.e., the optimal range is located in the intermediate part of the initial range), yet the exact ranges still vary considerably across investigations (e.g., Clos et al. 2013; Bzdok et al. 2015; Wang et al. forthcoming).

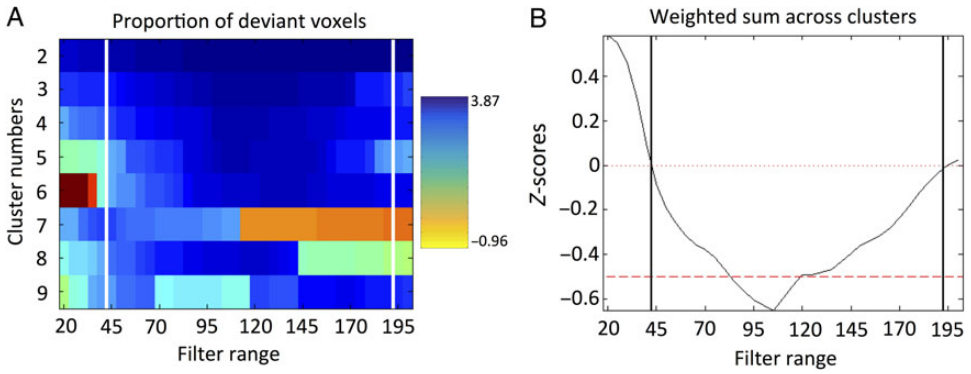

Figure 3. (*A*) Illustration of the consistency in the assignment of individual voxels to clusters as a function of the filter size and the number of clusters. Warm colors indicate high numbers of deviant voxels (i.e., instable solutions) and cold colors indicate a low number of deviant voxels (i.e., stable solutions). The vertical line represents the ultimately selected filter range that yielded the most stable clustering. (*B*) Z-scores on median filtered deviants (normalized for *K*).

Selection of the Optimal Cluster Solution

In the following series of analyses, the optimal number of K clusters was determined based on the evaluation of several cluster quality criteria. These analyses were restricted to the optimal filter range, defined in the previous step. To reveal the optimal number of clusters, we examined a combination of topologic, information theoretic, and cluster separation characteristics of the different cluster solutions. Importantly, each of these metrics captures different aspects of the quality of the cluster separation, and the selection of an optimal solution should thus be based on convergent evidence across metrics.

The first topologic criterion was the *percentage of misclassified voxels*. This criterion indicates the stability of a cluster solution across different filter sizes. Specifically, it reflects the proportion of voxels that are assigned to a different cluster compared with the most frequent assignment (i.e., the cluster mode) across all filter sizes. This indirectly reflects the amount of noise and potentially local effects in the clustering. A good solution K is indicated by a percentage that is not significantly higher than that of the previous $K-1$ solution, especially if the subsequent $K+1$ solution leads to a significant increase.

Second, we examined the *percentage of voxels not related to the dominant parent cluster*, when compared with the $K-1$ solution. This metric, which is related to the hierarchy index (Kahnt et al. 2012), indicates the number of voxels that are lost when only voxels are considered that are consistent in hierarchy (compared with the previous solution). For example, with $K=3$, voxels assigned to Cluster 3 would be excluded if they were previously assigned to Cluster 2 (with $K=2$) and the majority of voxels in Cluster 3 actually stemmed from Cluster 1 (with $K=2$). A good solution K is indicated by a percentage of lost voxels that is lower than the median across all solutions, and that represents a local minimum (i.e., the percentage is lower than those of the previous $K-1$ solution and the subsequent $K+1$ solution).

Third, as a information theoretic criterion, we examined the *variation of information* metric [VI; see Meila (2007)]. The VI assesses the similarity of cluster assignments, based on their mutual information, and has been used before in determining the optimal numbers of subdivisions of a brain region (Kelly et al. 2010; Kahnt et al. 2012). Here, we applied the VI metric in 2 contexts. First, we assessed the VI between filter sizes (i.e., 45–190 experiments) for each cluster number K. In this context, the VI indicates the stability of a cluster solution, indexed as its independence from a particular filter size. Good cluster solutions should not show an increase in VI, compared with the previous solution, and/or exhibit an increase with the subsequent solution. Second, we computed the VI across different numbers of K clusters (averaged across filter sizes). In this context, the VI indicates the amount of mutual information between neighboring cluster solutions. Good solutions are indicated by a significant increase in the VI when moving from the current solution K to the subsequent solution $K+1$ (primary criterion), and/or a decrease in VI when moving from the previous solution $K-1$ to the current solution K (secondary solution).

Finally, as a cluster separation criterion, we computed *silhouette values*. This score indicates, for each voxel, the similarity to voxels in the same cluster, when compared with voxels in other clusters. As the goal of cluster analysis is to obtain solutions with high intracluster similarity and low intercluster similarity, good solutions are indicated by silhouette values that are significantly higher than those in the $K-1$ solution, especially if the $K+1$ solution yields no further increase.

Importantly, every metric used captures different aspects of cluster separation quality. Hence, an optimal solution should be identified based on convergent evidence across metrics.

Illustration of the Optimal Cluster Solution

The application of the aforementioned cluster metrics consistently identified the two-cluster solution and the six-cluster solution as the most stable parcellations of the seed VOI, at different levels of detail (Fig. 4). All subsequent analyses were restricted to voxels that were hierarchically and spatially consistent and located in the gray matter. In addition, we used multidimensional scaling (MDS) to visualize the similarity of the different clusters, as measured by their whole-brain co-activation profiles (Fig. 7). MDS allows the visualization of N-dimensional data into a two-dimensional space. For each of the 30 optimal filter sizes (i.e., 45–190 experiments in steps of 5), we computed $N_s \times N_s$ matrices that indicate the correlation distances between the co-activation profiles of the respective seed voxels using the same distance metric as above (i.e., one minus the pairwise correlation). MDS was then performed on the eigenimage of these distance matrices using Sammon's nonlinear mapping as a goodness-of-fit criterion.

Shared and Distinct Co-Activation Patterns

After the parcellation of the VOI, we conducted follow-up meta-analytic co-activation modeling (MACM) analyses to reveal cluster-wise patterns of whole-brain co-activation. Thus, for each cluster, we first identified studies in the BrainMap database that contained at least one activation focus within the respective cluster borders using the same restrictions as described above (i.e., only "normal mapping" studies with healthy adults). Thereafter, an ALE meta-analysis was performed on the resulting number of experiments to reveal statistically significant convergence of co-activation. These meta-analyses were conducted analogously to the procedures described above, except that we now performed statistical inference on the resulting ALE maps. To this end, we compared the ALE maps of experiments associated with a given cluster with a null distribution that reflects a random spatial association between experiments with a fixed within-experiment distribution of foci [see Eickhoff et al. (2009)]. This random-effects inference reveals above-chance convergence between experiments rather than clustering of foci within experiments. The observed ALE scores were tested against this null distribution yielding a map of P-values (Eickhoff et al. 2012) that were transformed to z-values and thresholded (cluster-level: family-wise error-corrected $P<0.05$; voxel level: uncorrected $P<0.001$).

Upon completion of the cluster-wise MACM analyses, we performed a series of conjunction and contrast analyses to reveal commonalities and differences between the co-activation patterns of the clusters. We first conducted a minimum-statistic conjunction between the thresholded ALE maps of all clusters to reveal the overlap of co-activation patterns (Nichols et al. 2005; Caspers et al. 2010). Thereafter, we computed the voxel-wise differences between ALE maps to reveal statistically significant differences in co-activation patterns between all pairs of clusters (similar to Eickhoff et al. 2011). These difference maps were then compared with a null distribution. To generate this distribution, we pooled all experiments that contributed to either MACM analysis (i.e., all experiments associated with the 2 clusters) and assigned them randomly to 2 groups of equal size. ALE scores were then calculated for both groups and a voxel-wise difference test was conducted for each voxel. This procedure was repeated 10 000 times, yielding the final null distribution of the difference between the ALE scores of the MACM analyses of the 2 clusters. We then conducted a voxel-wise test of the observed difference map against this null distribution, yielding a posterior

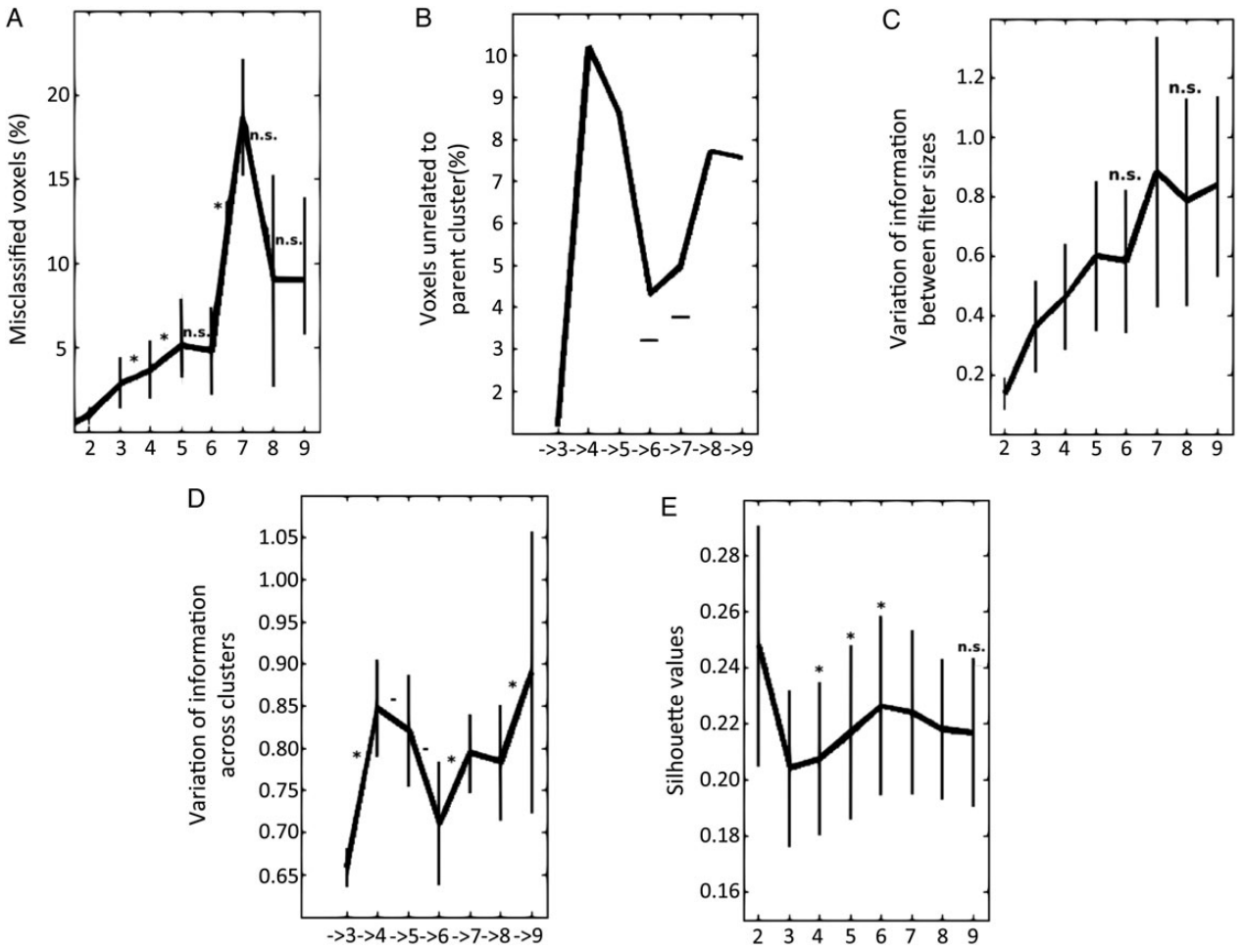

Figure 4. Cluster metrics that were used for the identification of the optimal solution K. (*A*) Percentage of misclassified voxels: The six-cluster solution is considered a good solution because it does not lead to a significant increase in the percentage of misclassified voxels (n.s.) when compared with the K – 1 solution, and the subsequent K + 1 solution yields a significant increase (asterisks). (*B*) Percentage of voxels that are not related to the parent cluster: The six- and seven-cluster solutions are considered good solutions because the percentages of lost voxels are lower than the median across all solutions (horizontal bar). (*C*) VI between filter sizes: The six- and the eight-cluster solutions are considered good solutions because they do not show an increase in VI compared with the previous solution (n.s.). (*D*) VI across cluster solutions: The six-cluster solution is considered the optimal solution because it displays a significant decrease in VI compared with the previous solution (–) and the subsequent solution leads to a significant increase in VI (asterisks). (*E*) Silhouette values: The six-cluster solution is considered the optimal solution, as it displays a significantly higher silhouette value than the previous solution (asterisks) and the subsequent solution leads to significant decrease. Each cluster metric is described in detail in the Materials and Methods section.

probability that an observed difference is not attributable to random noise. The resulting values were thresholded at $P > 0.95$ (i.e., a 95% chance that an observed difference reflects a true difference) and inclusively masked with the respective main effect (i.e., the significant effect of the MACM of the particular cluster). Finally, we sought to delineate the patterns of co-activation that are specific for each cluster. To this end, we calculated conjunction maps across the difference maps of a given cluster with all the other clusters, revealing voxels that exhibited significantly stronger co-activation with a particular cluster compared with all other clusters.

Functional Characterization

In the last set of analyses, we aimed at specifying the functional characteristics of the previously delineated clusters by examining the functional profiles of experiments that activate each cluster. To this end, we accessed the taxonomic categories "BD" and "PC" based on which studies in the BrainMap database are coded. BDs include the relatively broad categories "cognition," "action," "perception," "emotion," and "interoception" as well as their subcategories. PCs denote the specific tasks that were used (see http://brainmap.org/scribe for more details). To establish a functional characterization of differences between the final clusters, we quantified "forward inference" and "reverse inference" on the BDs and PCs of each cluster. *Forward inference* refers to the probability of observing activity in a particular brain region, given the knowledge of a psychological state (i.e., the consistency of a link between state and brain activation). Thus, in this approach, we determined a cluster's functional profile by identifying taxonomic labels for which the probability of activating a specific cluster was higher than by chance (i.e., across the entire database). This was achieved by the means of a binomial test ($P < 0.05$; Bonferroni-corrected for multiple comparisons) that assessed whether or not the conditional probability of the cluster's activation given a particular label [*P*(Activation|Task)] was higher than the baseline probability of activating that cluster per se [*P*(Activation)]. *Reverse inference*, on the other hand, refers to the

probability of a psychological state being present given the knowledge of a particular brain activation (i.e., the specificity of a link between state and brain activation). Thus, in this approach, we determined a cluster's functional profile by identifying the most likely BDs and PCs given the activation of a specific cluster. This likelihood $P(\text{Task}|\text{Activation})$ was derived from the previously used conditional probability $P(\text{Activation}|\text{Task})$ as well as the task's and the cluster's baseline probabilities $P(\text{Task})$ and $P(\text{Activation})$ using Bayes rule. Significance was established via a χ^2 test ($P < 0.05$, Bonferroni-corrected for multiple comparisons).

In a second series of post hoc analyses, we further specified the functional characterization of selected clusters using Neurosynth (www.neurosynth.org/). Neurosynth is another database for the large-scale analysis of neuroimaging data [see Yarkoni et al. (2011)] that is based on different conceptual principles than BrainMap [see Laird et al. (2013) and Fox et al. (2014) for comparison]. Instead of analyzing manually coded taxonomic labels, Neurosynth applies text-mining techniques to access frequency-based weightings of specific terms in published neuroimaging articles (e.g., "working memory," "pain," or "emotion") and relates them to the foci that are reported in the respective studies to derive meta-analyses [see Yarkoni et al. (2011) for an overview]. This "topic-mapping" approach permits to establish quantitative associations between particular terms and neuroanatomical locations. Two major types of analyses are implemented in the Neurosynth web interface: *Location-based* analyses reveal terms that are frequently used in studies that report activation at a particular brain region, and *term-based* analyses reveal brain regions that are associated with a particular search term. Both types of analyses can be quantified either in terms of consistency (forward inference) or in terms of specificity (reverse inference; see above). To further explore and validate the functional profiles of the ensuing clusters of our parcellation, we performed location-based searches (forward and reverse inference) using the peak coordinates of the respective clusters as input.

Results

Selection of an Optimal Filter Range

Analyzing the consistency of the cluster assignment for individual voxels across different filter sizes revealed that a range of 45–190 experiments produced the most stable results (see Fig. 3 above). Accordingly, all further analyses were based on this range of filter sizes.

Selection of an Optimal Cluster Solution

The subsequent application of topologic, information theoretic, and cluster separation metrics (see the Materials and Methods section) consistently identified both the two-cluster solution and the six-cluster solution as optimal parcellations of the VOI at different levels of detail (Fig. 4). In particular, the percentage of misclassified voxels exhibited 2 minima with the two-cluster solution and the six-cluster solution. That is, after monotonous increase from the 2 clusters up to the 5 clusters, the percentage did not increase further when moving to the six-cluster solution. In addition, the percentage was significantly lower than with the subsequent seven-cluster solution (Fig. 4A). A similar pattern was found for the *percentage of voxels that are not related to the parent cluster*. The proportion of lost voxels with the six-cluster solution was below the median across all 8 solutions, and it was significantly lower than with the preceding and the subsequent solutions (Fig. 4B). In the same vein, the *variation of information between filter sizes* increased monotonously from 2 up to 5 clusters where it reached a local maximum and numerically decreased with the six-cluster solution. Moving to the seven-cluster solution lead to a significant increase in the variation of information (Fig. 4C). The *variation of information across clusters* also identified the maximum of stability with the six-cluster solution, as indicated by a local minimum (Fig. 4D). Finally, *silhouette values* displayed a maximum with the two-cluster solution, followed by a drop when moving to the three-cluster solution. Subsequently, the values increased continuously from 3 up to 6 clusters, but additional clusters yielded no further increase (Fig. 4E). Taken together, the high degree of consistency among different topological, information theoretic, and cluster separation metrics provides very strong support for the parcellation of the VOI into either 2 or 6 clusters. Obtaining multiple solutions, at different levels of detail, that fit the data equally well is a common observation in parcellation studies and cluster analyses more generally [see, e.g., Yeo et al. (2011)]. As can be seen in Figure 5 and in the Supplementary material, the two-cluster solution cleanly separated the premotor sections of the seed regions from the prefrontal sections, whereas the six-cluster solution also revealed subdivisions within the LPFC. Given our focus on prefrontal cortex organization, we will focus primarily on the more detailed six-cluster solution here (see Supplementary material for an overview of the two-cluster solution). Moreover, note that although it is principally possible that cluster analyses with $K > 9$ would yield solutions with even better fit, the employed cluster metrics consistently indicate a decreasing fit with higher numbers of K.

Anatomical Description of Clusters

The locations of the 6 resulting clusters are illustrated in Figure 5 and Table 1. Cluster 1 was located at the posterior end of the IFS. It was situated deep in the cortex at the intersection of the inferior frontal and the inferior precentral sulci, spanning the adjacent parts of the precentral, inferior frontal, and MFG. The cluster's location and extent both correspond with previous anatomical definitions of the IFJ that were based on group or single-subject fMRI studies (Derrfuss et al. 2004, 2009). Cluster 2 was located on the precentral gyrus. It lay caudally and laterally of Cluster 1

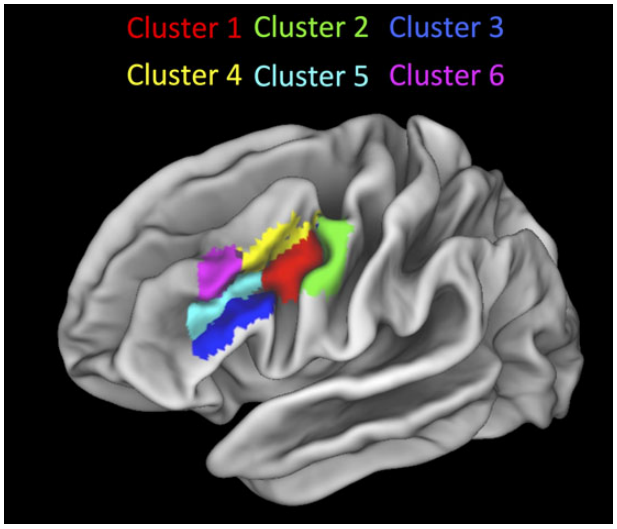

Figure 5. Anatomical location of the 6 clusters that resulted from the *K*-means clustering of the L IFS VOI.

and did not extend beyond the precentral sulcus. Cluster 3 was located on the inferior frontal gyrus (IFG), rostrally and ventrally of Cluster 1. It extended slightly on the adjacent IFS. Cluster 4 was located on the posterior end of the MFG. Ventrally it was delimited by the IFS, and caudally (in large parts) by the precentral sulcus. Cluster 5 was located deep in the more anterior parts of the IFS. The progression of this cluster followed the IFS in anterior direction. Finally, Cluster 6 was located in the anterior part of the MFG, directly rostral of Cluster 3 and dorsal of Cluster 5, at a location typically referred to as "mid-DLPFC."

We also examined the stepwise division of the seed region into the 6 ensuing clusters at different levels of *K*. This sequence is informative about the similarity among the different clusters and further illuminates the organization within the VOI from a different perspective. As can be seen in Figure 6*A*, at $K = 2$, the premotor section (Cluster 2) was separated from the remaining VOI and did not change further in the subsequent clustering steps. At $K = 3$, the IFG region (Cluster 3) was separated from the remaining anterior portion of the VOI and did not change further at subsequent clustering steps. At $K = 4$, the dorsolateral section of the VOI (i.e., Clusters 4 and 6) was dissociated from the remaining seed region. At $K = 5$, the anterior inferior frontal sulcus (aIFS) region (Cluster 5) was separated from the IFJ region (Cluster 1). Finally, at $K = 6$, the 2 sections along the MFG (Clusters 4 and 6) separated from one another. Overall, this separation sequence is consistent with the assumption that the clusters on the precentral gyrus and the IFG constitute rather distinct functional modules, when compared with the remaining clusters along the IFS and the MFG that differ only on a finer scale. This is also evident in the MDS results (Fig. 6*B*), which indicate a clear separation of Cluster 2 (PMC) and Cluster 3 (IFG) from the remaining VOI, whereas the co-activation profiles of Clusters 1 (IFJ), 4 (pMFG), 5 (aIFS), and 6 (mid-DLPFC) are much more similar.

Table 1 Overview of the size, anatomical location, and cytoarchitechtonic mapping of each cluster

Region	Label	Size	MNI coordinates		
			x	y	z
Cluster 1	IFJ	765	−37	5	31
Cluster 2	PMC	671	−52	2	39
Cluster 3	IFG	777	−51	25	21
Cluster 4	pMFG	539	−43	14	39
Cluster 5	aIFS	529	−36	25	19
Cluster 6	mid-DLPFC	385	−40	31	25

Note: MNI coordinates refer to the respective centers of gravity of each cluster. IFJ, inferior frontal junction; PMC, premotor cortex; IFG, inferior frontal gyrus; aIFS, anterior inferior frontal sulcus; pMFG, posterior middle frontal gyrus; mid-DLPFC, mid-dorsolateral prefrontal cortex.

Common and Specific Co-Activation Patterns

After the delineation of the 6 final clusters, we performed cluster-wise MACM analyses to reveal each clusters' whole-brain co-activation pattern (see the Materials and Methods section for details). The resulting thresholded ALE maps were used to identify both common and specific co-activation patterns. In the first step, we computed a conjunction analysis across all 6 MACM maps in order to reveal commonalities in co-activation patterns across the different clusters (Fig. 7 and Table 2). This analysis revealed 2 large clusters along the bilateral IFS that encompassed large parts of the adjacent inferior frontal, middle frontal, and precentral gyri as well as the insular cortices. In addition, there was a cluster in the medial frontal wall covering the supplementary motor area (SMA), pre-supplementary motor area (pre-SMA), and the anterior cingulate cortex (ACC), and another cluster along the left intraparietal sulcus (IPS). Taken together, these areas correspond well with previous descriptions of a fronto-parietal "cognitive control network" (Cole and Schneider 2007) or "multiple demand system" (Duncan 2010) that is implicated in the coordination of goal-oriented cognition and action.

Thereafter, we computed conjunction maps across each cluster's difference maps to reveal co-activation patterns that are specific for each cluster (see description in the Materials and Methods section). Cluster 1 (IFJ) exhibited specific co-activation with its right homotope, the pre-SMA, the left IPS, and the right anterior insula. For Cluster 2 (PMC), specific co-activation was found in 2 large bilateral clusters that covered the pre- and postcentral gyri. The left cluster extended to the parietal lobe, covering the supramarginal gyrus (SMG) and the anterior IPS. In addition, there was specific co-activation in the medial frontal wall in the SMA, and bilaterally in the putamen and the thalami. Finally, there were 2 additional clusters on the temporal lobe. One covered the left superior and middle temporal gyri, and the other one was located on the right temporal pole. Cluster 3 (IFG) displayed specific co-activation with large parts of the left IFG, as

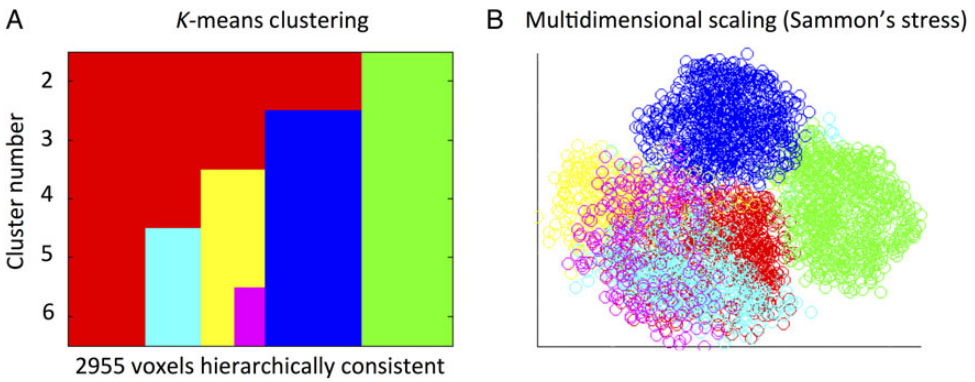

Figure 6. Illustration of the best cluster solution ($K = 6$). (*A*) Pattern of cluster assignment and cluster splitting at different levels of *K*. (*B*) Visualization of the six-cluster solution by the means of multidimensional scaling. The axes represent dimensionless factors representing the two-dimensional projection of the data. Points represent voxels and their proximity indicates the similarity of their co-activation profiles. Color coding: red = Cluster 1, green = Cluster 2, blue = Cluster 3, yellow = Cluster 4, cyan = Cluster 5, violet = Cluster 6.

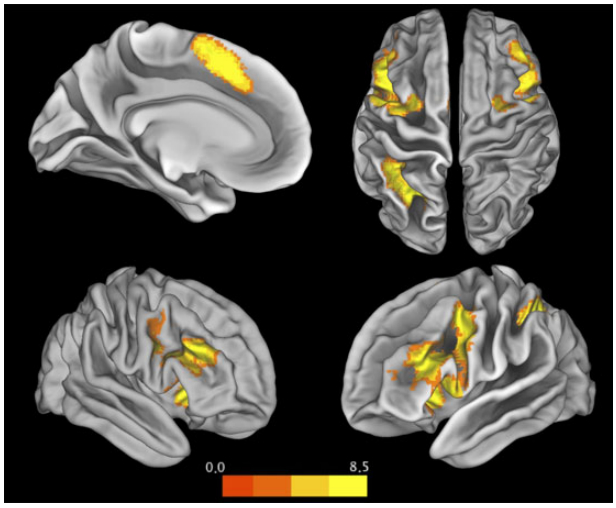

Figure 7. Conjunction map of the co-activation patterns across all 6 clusters.

Table 2 Overview of the conjunction analysis across the co-activation maps of all 6 clusters

Region	Size	MNI coordinates		
		x	y	z
L IFS	4383	−43	16	21
R IFS	2787	43	20	21
MFC	188	10	16	48
L IPS	1579	−34	−54	46

Note: MNI coordinates refer to the respective centers of gravity and the cluster size is indicated in the number of voxels.
IFS, inferior frontal sulcus; MFC, medial frontal cortex; IPS, intraparietal sulcus.

well as with 2 clusters located on the left middle and inferior temporal gyri (MTG, ITG). For Cluster 4 (pMFG), there was a single focus of specific co-activation, located in the left posterior inferior parietal lobule (IPL). Cluster 5 (aIFS) exhibited specific co-activation with its right homotope and with the rostral anterior cingulate cortex (ACC). Finally, for Cluster 6 (mid-DLPFC), specific co-activation was found within its right homotope, as well as bilaterally on the medial IPL. Figure 8 and Table 3 illustrate the specific co-actication patterns of all 6 clusters.

Functional Characterization

To examine functional characteristics of the different clusters, we employed a post hoc analysis of the functional profiles of experiments that activate each cluster. To this end, we quantified forward and reverse inference of BDs and PCs separately for each cluster (see the Materials and Methods section). Of note, this inference is constrained by the taxonomy and categorization scheme of the BrainMap database and should therefore be considered as explorative. Overall, the data confirmed the strong link between the left frontal lobe and linguistic functions, as reflected in the frequent and strong association of language-related categories with all 6 clusters. In addition, some marked differences in the clusters' profiles were evident. In brief, Cluster 2 was strongly related with action processing, both action execution as well as action observation and imagination. Cluster 3 showed the strongest association with language and semantic memory. Finally, Clusters 1, 4, 5, and 6 all showed a reliable association with tasks requiring cognitive control across a rather wide array of subprocesses, including conflict resolution (Stroop task), flexibility (task-switching or Wisconsin card sorting test), and working memory (*n*-back task), with little evidence for pronounced differences between the clusters (see Supplementary Figs 1 and 2 for a complete overview).

In the next step, we further specified the functional characterization of Cluster 1 (IFJ), Cluster 5 (aIFS), and Cluster 6 (mid-DLPFC) using a location-based topic-mapping analysis via Neurosynth (see the Materials and Methods section). We focused on these 3 clusters because they correspond most closely to activation foci in the cognitive control literature and are often treated similarly. As in the previous analyses, we examined both forward inference and reverse inference to reveal the consistency and the specificity links between the clusters and functions, as reflected in the respective terms (see the Materials and Methods section). Replicating the previous set of analyses, all 3 clusters exhibited strong links with both executive and linguistic functions. Yet, with regard to control functions, subtle differentiations were evident between the clusters' profiles. The IFJ cluster was primarily associated with functions related to the selection and specification of task demands (e.g., "task-relevant," "stop", "congruency", "rules", or "contextual"). The aIFS cluster, on the other hand, was most strongly associated with functions related to interference resolution (e.g., "competition," "task-irrelevant," and "violations") and attention shifts (e.g., "shifting," or " switching"). Finally, the mid-DLPFC cluster clearly showed the strongest link to working memory (e.g., "1-back," "2-back," "*n*-back," and "visuospatial") and higher-order planning functions (e.g., "maintenance," planning," "preparation," and "task-irrelevant"; see Supplementary Tables 1 and 2 for a complete overview).

External Validation

In the last series of analyses, we sought to validate our parcellation of the IFJ (Cluster 1) with independent data. To this end, we compared this cluster with several parcellation schemes and coordinates from the literature. Only the IFJ cluster was subjected to these analyses, as the outer boundaries of the adjacent clusters are likely incomplete due to the arbitrary boundaries of our seed region (see the Materials and Methods section). We first examined the parcellation by Neubert et al. (2014). As mentioned above, this study employed a combination of RSFC and diffusion-weighted imaging to identify the subdivision of the ventrolateral frontal cortex. In this study, a cluster was identified at the caudal end of the IFS, directly rostral to the precentral gyrus, which was similarly labeled as IFJ. As can be seen in Figure 9A, the 2 clusters showed good overlap, which was confirmed by a Dice coefficient of 0.58. The cluster from the present study extended slightly further caudally, though it covered the adjacent ventral premotor cortex (displayed in green) only minimally. Next, we examined the parcellation by Yeo et al. (2011). This study subdivided the entire neocortex based on cluster analyses of RSFC data, yielding one large cluster along the entire IFS. Figure 9B shows that Cluster 1 from the present study cleanly matched into the caudal end of this IFS region, in particular at the caudal and dorsal transitions to the precentral gyrus and MFG, respectively. Finally, we examined the parcellation by Gordon et al. (2014) who employed RSFC-boundary mapping to the entire neocortex. As shown in Figure 9C, they identified 3 parcels along the IFS in rostrocaudal orientation. The most caudal parcel overlapped with Cluster 1 from the present study. In

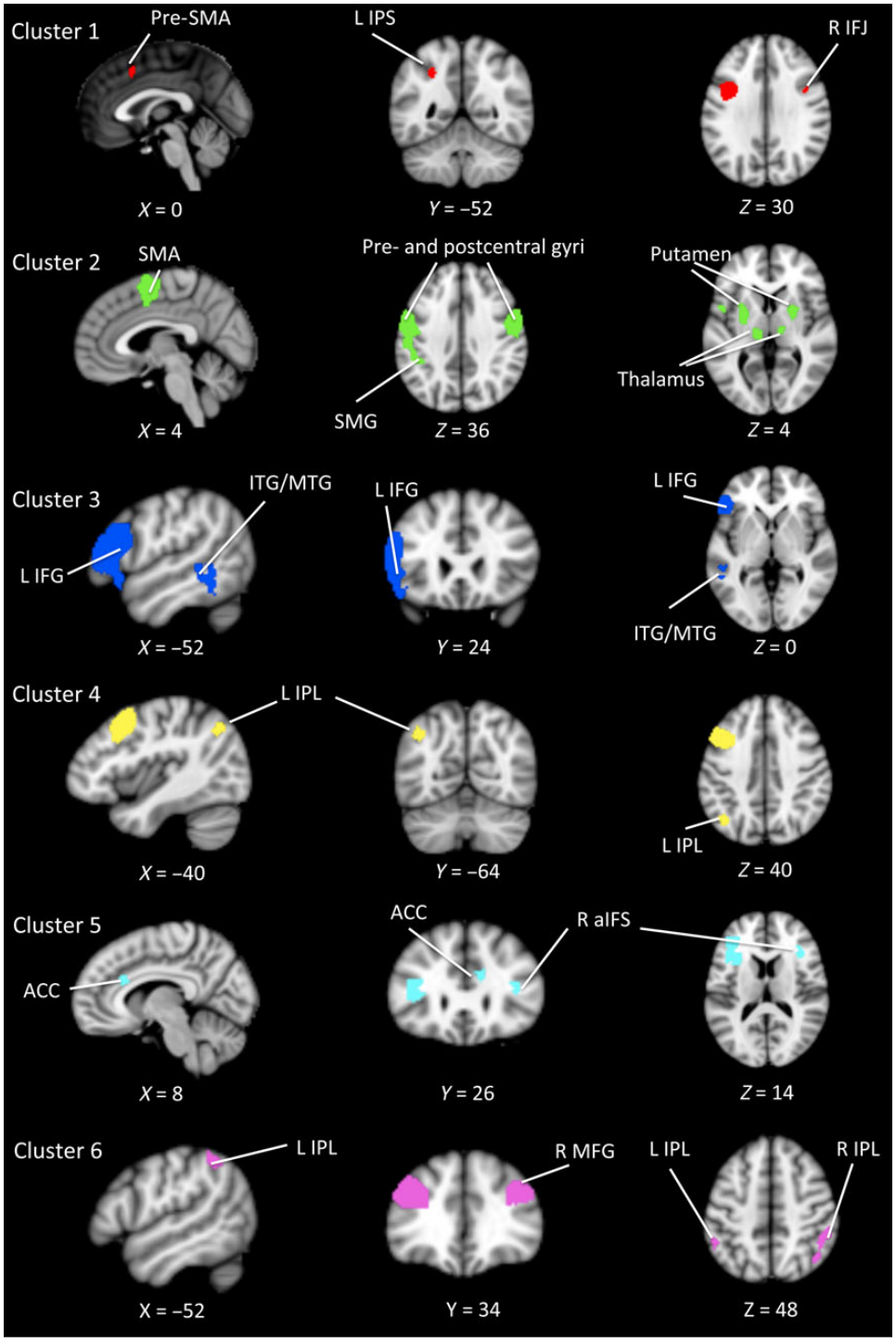

Figure 8. Specific patterns of co-activation for each cluster (i.e., regions that show significantly stronger co-activation with a given cluster than with all other 5 clusters). Patterns for the Clusters 1–6 are displayed from top to bottom.

particular, the dorsal boundary to the caudal MFG, the rostral boundary to the intermediate IFS parcel, and the caudal boundary to the precentral gyrus aligned closely. Overall, therefore, the IFJ cluster from our study matched well with existing parcellation schemes of the LPFC. As the latter were derived from differing data modalities and with different parcellation criteria, this corroborates the validity and functional anatomical plausibility of our results. Differences between parcellations were evident primarily with regard to ventral boundaries, which were more dorsal in our cluster and that by Neubert et al. (2014) compared with the schemes by Yeo et al. (2011) and Gordon et al. (2014). Although only speculative at this point, this may reflect methodological differences across investigations (e.g., between seed-based and non-seed-based analyses).

Table 3 Overview of specific co-activation patterns of each cluster

Region	Size	MNI coordinates		
		x	y	z
Cluster 1				
L IFJ	764	−38	4	32
R IFJ	96	42	9	27
Pre-SMA	131	2	17	46
L IPS	253	−27	−58	43
R anterior insula	101	34	28	−3
Cluster 2				
L pre- and postcentral gyri/SMG	2954	−49	−8	37
R pre- and postcentral gyri	1710	51	1	36
SMA/pre-SMA	1270	−1	2	55
L SPL	142	−32	−51	59
L Putamen	350	26	0	1
R Putamen	177	25	3	4
L Thalamus	330	−10	−22	3
R Thalamus	137	12	−18	8
L STG/MTG	157	−55	−38	14
R Temporal pole	73	52	10	−8
Cluster 3				
L IFG	1530	−50	26	9
L ITG/MTG	96	−52	−46	−9
Cluster 4				
L pMFG	1530	−41	14	43
L IPL	137	−40	−65	41
Cluster 5				
L IFS	811	−37	27	14
R IFS	129	39	26	14
R ACC	106	8	25	25
Cluster 6				
L MFG	944	−38	34	29
R MFG	794	40	37	27
L IPL	93	−50	−48	49
R IPL	464	48	−49	47

SPL, superior parietal lobule; STG, superior temporal gyrus.

In the final set of validation analyses, we compared our parcellation of the IFJ with different paradigm-based meta-analyses of executive functions from the literature. This confirmed that foci related to different control functions were located within the boundaries of the IFJ cluster, including task-switching (Derrfuss et al. 2005; located at −40, 4, 30; Niendam et al. 2012; located at −38, 6, 28), Stroop interference (Derrfuss et al. 2005; located at −40, 4, 32), response inhibition (Niendam et al. 2012; 2 peaks located at −42, 4, 32; and at −44, 6, 26; Levy and Wagner 2001; located at −46, 10, 28), and working memory (Niendam et al. 2012; located at −42, 16, 24; Rottschy et al. 2012; located at −46, 10, 26). Altogether, these results support the existence of a "core" IFJ region at the caudal and dorsal end of the IFS that possesses unique functional connections and contributes to a variety of cognitive demands.

Discussion

In the present study, we conducted a CBP of the left IFS and its adjacent sections within the LPFC. Our results show that a single IFJ region can be distinguished from neighboring areas on the basis of specific whole-brain co-activation patterns. Moreover, our data specify the IFJ's borders to the premotor cortex, the IFG, and the aIFS/mid-DLPFC. We discuss in the following section how our findings elucidate the role of the IFJ in human cognition, the organization of cognitive control functions in the frontal lobe, and the relationship between control and language in the left LPFC.

The IFJ as a Distinct Module in the LPFC

Our finding that the IFJ can be identified on the basis of a specific pattern of whole-brain co-activation solidifies the hypothesis that this brain region constitutes a core functional unit within the human frontal lobe [see Brass, Derrfuss, et al. (2005)]. This notion was further substantiated by the correspondence of the IFJ cluster with different parcellations from the literature, especially the one by Neubert et al. (2014). These parcellations converged not only in terms of location and extent, but also yielded very similar connections of the IFJ region (including pre-SMA, anterior insula, and the IPS). Our data therefore strongly imply that there is a core IFJ region that possesses specific anatomical and functional connections. This may serve as a template for future neuroimaging studies and help elucidating whether or not a given focus is likely to be located in the IFJ.

Importantly, the resulting borders between the IFJ and neighboring areas, along with the co-activation profiles of these regions, were anatomically plausible and converge with the existing literature. Caudally, the IFJ was dissociated from a cluster that occupied large parts of the premotor cortex (Cluster 2). This cluster exhibited specific co-activation with the SMA, the left anterior IPS/SMG, bilateral putamen and thalami, and showed a clear involvement in basic motor control functions. This finding is consistent with a large body of literature on a parietal–premotor network involved in action planning (Jeannerod et al. 1995; Wise et al. 1997; Rushworth et al. 2003; Desmurget and Sirigu 2009) and RSFC delineations of a "sensorimotor network" (Smith et al. 2009; Power et al. 2011). Ventrally, the IFJ bordered a cluster that extended on the IFG (Cluster 3). This cluster exhibited specific co-activation with the ITG/MTG and showed a strong link with linguistic and semantic processing, largely matching the locations reported in recent meta-analyses on language production and semantic memory (Vigneau et al. 2006; Binder et al. 2009; Clos et al. 2013). Finally, the IFJ could also be distinguished from more rostral regions in the vicinity of the IFS that were also implicated in cognitive control. One of these clusters was located more dorsally on the posterior end of the MFG and exhibited specific co-activation with the left posterior IPL (Cluster 4). Interestingly, this resembles 2 recent investigations that have identified very similar regions as being functionally connected both during memory retrieval (Nelson et al. 2010) and in the resting state (Power et al. 2011). Thus, although these regions do not constitute a commonly described network, they seem to form a replicable module that should be further examined with future research. Another cluster (Cluster 5) was located rostrally of the IFJ within the aIFS. This cluster was specifically co-activated with its right homotope and the ACC, and showed a clear involvement in cognitive control functions, most clearly in aspects related to the resolution of cognitive interference. The distinction of the aIFS from the IFJ is relevant, as a number of studies have reported parallel foci in both of these regions (e.g., Zysset et al. 2001; Ruge and Wolfensteller 2010; Kuo et al. 2014; Bahlmann et al. 2015). Our finding indicates that this may reflect activity in 2 related but nonetheless distinct cortical entities (see also the next section). The specific co-activation of the aIFS cluster with the ACC is also of interest. Notably, although both cingulate and frontolateral cortices are generally considered pivotal regions for control, current accounts make rather different assumptions about their respective contributions. Some frameworks emphasize their similarity in dynamically coding task-relevant variables (e.g.,

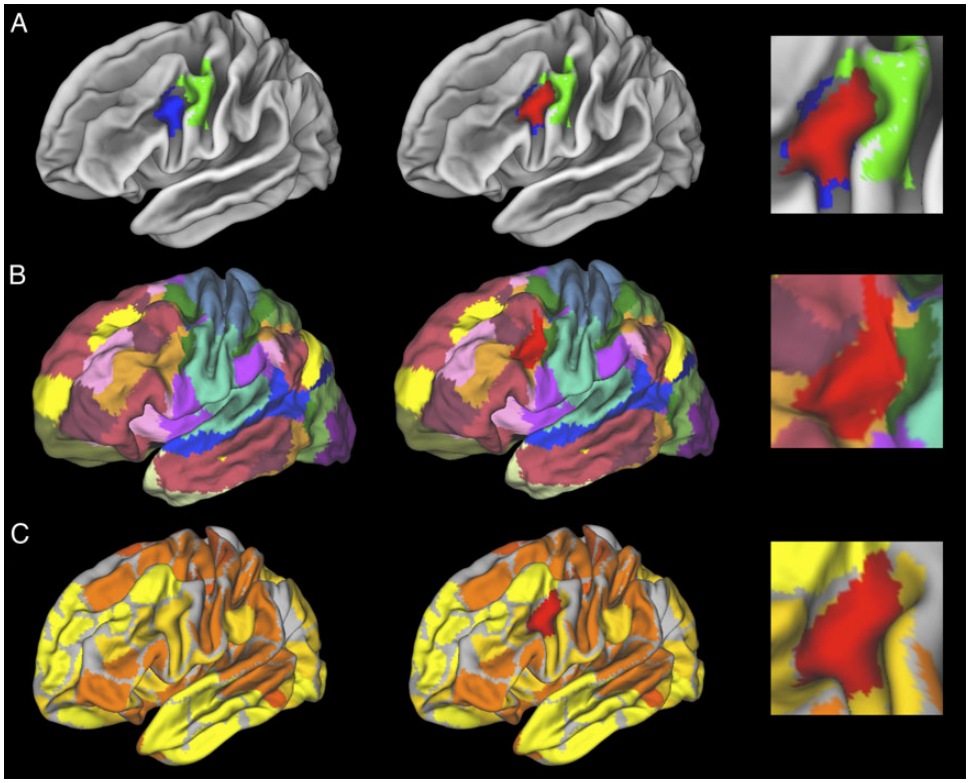

Figure 9. Comparison of Cluster 1 in the present study with existing parcellation schemes. (*A*) Parcellation of the IFJ (blue) and ventral premotor cortex (green) by Neubert et al. (2014). (*B*) Parcellation of the neocortex by Yeo et al. (2011). (*C*) Parcellation of the neocortex by Gordon et al. (2014). Note: Figures on the left shows the clusters/parcels from the respective studies alone. Figures in the middle display Cluster 1 from the present study (red) overlaid on the respective parcellation. Figures on the right display in high resolution the overlap between the cluster from the present study and the respective external parcellation schemes.

Duncan 2010), while others have proposed that they serve rather complementary roles, for example, in detecting interference and implementing top-down control (Botvinick et al. 2001) or in generating task control signals at different time scales (Dosenbach et al. 2008). Our results do not permit to distinguish between these accounts, but the finding of ACC–LPFC co-activation itself, along with the functional characterization, underscores the involvement of both regions in overcoming cognitive interference via adjustments of top-down control. Finally, we identified a cluster that was located on the more rostral sections of the MFG, rostral to Cluster 4 and dorsal to Cluster 5, corresponding to classical mid-DLPFC locations from the working memory and conflict control literature (e.g., MacDonald et al. 2000; Bunge et al. 2002; Braver et al. 2003; Curtis and D'Esposito 2003; Feredoes et al. 2011; Nee and Brown 2012, 2013). The specific co-activation of this cluster with the bilateral medial IPL nicely aligns with a number of findings that similarly observed enhanced coupling between DLPFC and the IPL, as opposed to stronger coupling between the IPS and more posterior LPFC regions such as the IFJ (e.g., Dosenbach et al. 2006, 2007; Neubert et al. 2014).

Toward a Taxonomy of Frontal Lobe Functions

Despite the clear anatomical delineation of the IFJ, the functional differentiation of this area from more rostral regions (i.e., aIFS and mid-DLPFC) proved challenging. All 3 clusters were shown to be generally associated with classical cognitive control tasks (e.g., the Stroop task, the *n*-back task, or the Wisconsin Card Sorting Test) and—to different extents—with linguistic functions (see the section below for further discussion). On the one hand, this high degree of similarity could be taken as support for adaptive coding or global workspace models that assume the entire IFS to be involved in general purpose problem-solving functions (e.g., Dehaene et al. 1998; Duncan and Owen 2000; Duncan 2010, 2013). On the other hand, this result may also reflect that the currently available taxonomic labels lack the specificity that is necessary to capture subtle differences between the functions of LPFC subregions. As noted above, it is questionable to what extent our current terminology maps onto the computations of the human brain (Poldrack 2006). Finally, it is also conceivable that the subregions along the IFS make distinct contributions to common overarching control functions, and are thus commonly activated by the same experimental paradigms. The text-mining-based post hoc analyses yielded some explorative evidence in favor of this interpretation: While the aIFS and the mid-DLPFC were most strongly associated with working memory and resolving interference from *task-irrelevant* information, the IFJ exhibited a more general association with contextual rules and the selection of *task-relevant* information. Interestingly, a similar distinction has been made in the working memory literature. Feredoes et al. (2011) recently proposed that the DLPFC "plays a role in target protection (. . .) whereas the inferior frontal junction plays a role in distinguishing relevant from irrelevant information for encoding" (p. 17513). A somewhat related distinction has been made by Dosenbach et al. (2006, 2007, 2008). Based on patterns of RSFC and meta-analyses of different types of control signals (i.e., start-cue related, sustained throughout the block, and error-related) across a large set of different tasks, they proposed that the IFJ (labeled "dFC" or "frontal cortex") is involved in processes of cue interpretation and task initiation, whereas the DLPFC contributes

more specifically to dynamic adjustments in control settings during task performance. A final difference between the aIFS/DLPFC and the IFJ that has been documented in the literature is that only the latter is subject to severe capacity limitations (Dux et al. 2006, 2009; Tombu et al. 2011; Todd et al. 2011) and contributes to both exogenous and endogenous control of attention (Asplund et al. 2010). Hence, the most plausible interpretation at the current stage is that the IFJ serves as a central bottleneck at the interface of bottom-up and top-down processing, whereas more rostral DLPFC regions participate more generally in top-down control to enforce task goals against external interference.

Co-Organization Principles Within Frontal and Parietal Cortices

From a broader perspective, our findings also contribute to theorizing on the organization principles of the frontal lobe. Gradient theories posit that the frontal cortex is organized into distinct modules along its rostrocaudal axis, with more rostral regions serving increasingly abstract or "higher-order" control functions (e.g., Koechlin and Summerfield 2007; Badre 2008). While the earliest versions of gradient theories were primarily concerned with the LPFC, recent work has indicated that a similar gradation may exist within the medial frontal wall (Kouneiher et al. 2009; Kim et al. 2011; De Baene et al. 2012), possibly reflecting the interplay between motivational and evaluative functions of the MFC and executive functions of the LPFC [see Kouneiher et al. (2009)]. Our results concur with these observations in revealing systematic patterns of mediolateral co-activation along the rostrocaudal axis of the frontal lobe. Most caudally, specific co-activation was found between the SMA and bilateral premotor cortices. This corresponds nicely with the network of areas that has typically been implicated in concrete "first-order" control, that is, action selection in response to the identity of concrete stimuli. In the intermediate parts of our seed region, specific co-activation was evident between the pre-SMA and bilaterally in the IFJ. This is also in accord with a network of areas that has been linked to contextual "second-order" control, that is, action control based on contextual rules that specify the behavioral relevance of stimulus features. Finally, in the most rostral part of the IFS, we observed co-activation of the ACC and the aIFS. This roughly corresponds to areas implicated in abstract "third-level" control, that is, the guidance of behavior based on temporally distal and/or dimensionally complex rules. However, it must be noted that the frontolateral component of this network is sometimes located more dorsally and could match more closely with Cluster 6 from our analysis.

An additional and novel observation in our data is that the different frontal networks exhibited specific patterns of co-activation with the parietal lobe. The caudal SMA–premotor network exhibited specific co-activation with the left anterior IPS/SMG, a region that has been strongly linked with motor attention (Rushworth, Ellison, et al. 2001; Rushworth, Krams, et al. 2001; Rushworth et al. 2003). The intermediate pre-SMA/IFJ network exhibited specific co-activation with the left medial IPS. This part of the IPS has been implicated in visuomotor transformations (Grefkes et al. 2004), and updating of context-dependent stimulus–response contingencies (Corbetta and Shulman 2002; Brass, Ullsperger, et al. 2005; Donsenbach et al. 2007; Muhle-Karbe, Andres, et al. 2014). No specific parietal co-activation was observed for the rostral ACC/aIFS network. As noted above, this might be related to the spatial uncertainty of the frontolateral component and the medial IPL, specifically co-activated with Cluster 6, could be seen as a parietal candidate region for more abstract components of control. Thus, in summary, our data not only confirm recent observations of parallel rostrocaudal gradients in the lateral and medial frontal lobes, but also indicate that the frontal gradation might correspond to specific subregions in the parietal cortex (see Fig. 10 for an illustration). In particular, the latter observation should be scrutinized more directly in future studies.

Note, however, that co-activation between specific subregions in the frontal and the parietal lobes should not be taken to imply that these regions serve equivalent functions. For example, we have recently shown, by means of transcranial magnetic stimulation (TMS), that the left IFJ and the left IPS make distinct causal contributions to task-switching, despite the robust co-activation of these areas in fMRI studies (Muhle-Karbe, Andres, et al. 2014). Specifically, while TMS over the IFJ interfered with shifting between abstract goals for stimulus categorization, TMS over the IPS perturbed the selection of more concrete stimulus-response mapping rules. Accordingly, co-activation between frontal and parietal subregions during complex tasks likely reflect highly related but nevertheless dissociable functions.

Cognitive Control and Language in the Left LPFC

A final aspect of our data pertains to the co-existence of linguistic and executive functions in large parts of our seed region. The strongest link with language was observed in Cluster 3 that

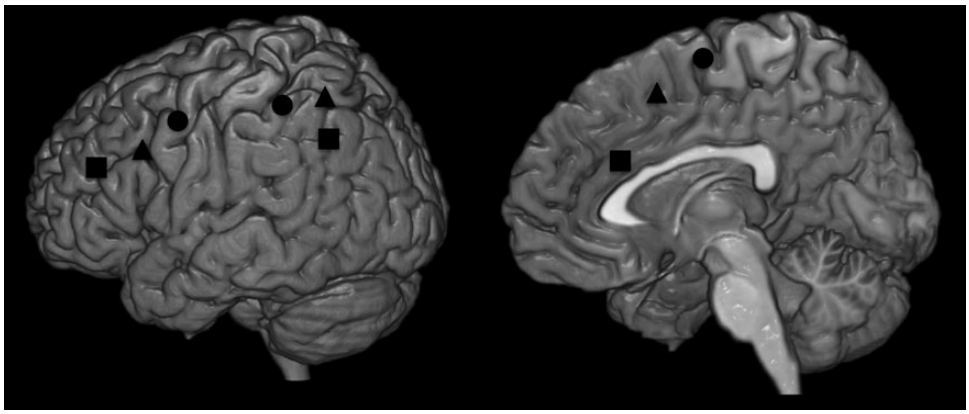

Figure 10. Schematic illustration of functional gradients in frontolateral, frontomedian, and parietal cortices. Circles refer to concrete "first-order" control functions, triangles refer to intermediate "second-order" control functions, and squares refer to abstract "third-order" control functions (see text for details). Note that the parietal component of third-order control is based on the specific co-activation of Cluster 6.

included the dorsal part of Broca's region. However, associations with linguistic functions were also found in the more dorsal areas along the IFS that are typically implicated in abstract cognitive control processes. This result is interesting given the ongoing debate in the literature on the relation between language and control (e.g., Hagoort 2005; Koechlin and Jubault 2006; Fedorenko et al. 2012). One possible interpretation of our data would be that language and control rely on shared mechanisms, at least under particular conditions. In line with this view, control-related brain activity is often left-lateralized when tasks include verbal stimulus material (e.g., Kouneiher et al. 2009; Asplund et al. 2010; De Baene et al. 2012; Rottschy et al. 2012), linguistic categorizations (Stephan et al. 2003), or when self-verbalization is an adaptive strategy for task performance [see Gruber and Goschke (2004)]. Thus, left-lateralized LPFC regions might serve control functions in the service of linguistic information coding, whereas non-linguistic attentional capacities might be more right-lateralized (e.g., Mesulam 1981; Corbetta and Shulman 2002; Cai et al. 2012). Alternatively, however, the neural overlap of language and control functions in our study could also result from methodological constraints. For instance, low-level baseline contrasts in language studies might confound linguistic and control demands. Likewise, the averaged group data that were input to our analyses could mask a more fine-scaled modularization that is evident only at the level of individual subjects (Fedorenko et al. 2010). In any event, more research will be necessary to disambiguate the relation between the neural bases of language and control in the left frontal lobe.

Limitations and Future Directions

Although our parcellation was consistently supported both by the employed cluster metrics and the parcellation's concordance with external data, it should be emphasized that it does not reflect a conclusive or "correct" parcellation of the L IFS seed region for several reasons. First and foremost, our study aimed at delineating the IFJ within its cortical environment and the seed region was designed for this purpose. This allowed us to characterize the transition from the IFJ to adjacent areas in different directions, but the outer boundaries of these areas are unlikely to be conclusively mapped in our study. Second, the frontal lobe in particular can be subdivided on the basis of diverse modalities and criteria (e.g., cortico-cortical connections, cortico-striatal projections, attended sensory modality, level of abstraction, and cytoarchitecture) and the resulting schemes will inevitably depend to some degree on these choices [see Amunts et al. (2014) and Bertolero and D'Esposito (2014) for discussion]. Accordingly, our findings only provide the optimal scheme for the chosen modality and future research must determine its generalizability. Finally, future studies should also examine to what extent our scheme applies to the right hemisphere and if a right IFJ can be identified in a similar manner.

Conclusion

In the present study, we conducted a CBP of the left posterior LPFC to delineate the IFJ from neighboring brain areas on the basis of specific whole-brain co-activation patterns. Our results strengthen the idea that the IFJ constitutes a core functional unit within the frontal lobe and delineate the transition from this area to adjacent parts of the LPFC. More generally, our study underscores the usefulness of meta-analytic techniques in revealing modularization in the human brain.

Supplementary Material

Supplementary material can be found at: http://www.cercor.oxfordjournals.org

Funding

This work was supported by grant B/09019/02 of the Flemish Research Foundation (FWO; P.S.M.-K. and M.B.), grants EI 816/4-1, EI 816/6-1, and LA 3071/3-1 of the German Research Foundation (DFG; S.B.E.), the Human Brain Project of the European EFT program (S.B.E.), grant R01-MH074457 from the National Institute of Mental Health (S.B.E.), and a Christopher Welch Scholarship (F.X.N.).

Notes

Conflict of Interest: None declared.

References

Amunts K, Hawrylycz MJ, Van Essen DC, Van Horn JD, Harel N, Poline J-B, De Martino F, Bjaalie JG, Dehaene-Lambertz G, Dehaene S, et al. 2014. Interoperable atlases of the human brain. Neuroimage. 99:525–532.

Amunts K, Lenzen M, Friederici AD, Schleicher A, Morosan P, Palomero-Gallagher N, Zilles K. 2010. Broca's region: novel organization principles and multiple receptor mapping. PLoS Biol. 8:1–16.

Asplund CL, Todd JJ, Snyder AP, Marois R. 2010. A central role for the lateral prefrontal cortex in goal-directed and stimulus-driven attention. Nat Neurosci. 13:507–512.

Badre D. 2008. Cognitive control, hierarchy, and the rostro-caudal organization of the frontal lobes. Trends Cogn Sci. 12:193–200.

Badre D, D'Esposito M. 2007. Functional magnetic resonance imaging evidence for a hierarchical organization of the prefrontal cortex. J Cogn Neurosci. 19:2082–2099.

Badre D, D'Esposito M. 2009. Is the rostro-caudal axis of the frontal lobe hierarchical? Nat Rev Neurosci 10:659–669.

Bahlmann J, Aarts E, D'Esposito M. 2015. Influence of motivation on control hierarchy in the human frontal cortex. J Neurosci. 35:3207–3217.

Baldauf D, Desimone R. 2014. Neural mechanisms of object-based attention. Science. 344:424–427.

Bertolero M, D'Esposito M. 2014. There is no "best" brain parcellation for complex brain networks—one parcellation is not sufficient [abstract]. Soc Neurosci. 838.01/RR13.

Binder JR, Desai RH, Graves WW, Conant LL. 2009. Where is the semantic system? A critical review and meta-analysis of 120 functional neuroimaging studies. Cereb Cortex. 19:2767–2796.

Botvinick M, Braver TS, Barch DM, Carter CS, Cohen JD. 2001. Conflict monitoring and cognitive control. Psych Rev. 108:624–652.

Brass M, Derrfuss J, Forstmann B, von Cramon DY. 2005. The role of the inferior frontal junction area in cognitive control. Trends Cogn Sci. 9:314–316.

Brass M, Ullsperger M, Knoesche TR, von Cramon DY, Phillips NA. 2005. Who comes first? The role of the prefrontal and parietal cortex in cognitive control. J Cogn Neurosci. 17:1367–1375.

Brass M, von Cramon DY. 2004a. Decomposing components of task preparation with functional magnetic resonance imaging. J Cogn Neurosci. 16:609–620.

Brass M, von Cramon DY. 2002. The role of the frontal cortex in task preparation. Cereb Cortex. 12:908–914.

Brass M, von Cramon DY. 2004b. Selection for cognitive control: a functional magnetic resonance imaging study on the selection of task-relevant information. J Neurosci. 24:8847–8852.

Braver TS, Reynolds JR, Donaldson DI. 2003. Neural mechanisms of transient and sustained cognitive control during task switching. Neuron. 39:713–726.

Bunge SA, Hazeltine E, Scanlon MD, Rosen AC, Gabrieli JDE. 2002. Dissociable contributions of prefrontal and parietal cortices to response selection. Neuroimage. 17:1562–1571.

Bunge SA, Kahn I, Wallis JD, Miller EK, Wagner AD. 2003. Neural circuits subserving the retrieval and maintenance of abstract rules. J Neurophysiol. 90:3419–3428.

Bzdok D, Heeger A, Langer R, Laird AR, Fox PT, Palomero-Gallagher N, Vogt BA, Zilles K, Eickhoff SB. 2015. Subspecialization in the human posterior medial cortex. Neuroimage. 106:55–71.

Bzdok D, Laird AR, Zilles K, Fox PT, Eickhoff SB. 2013. An investigation of the structural, connectional, and functional subspecialization in the human amygdala. Hum Brain Mapp. 34:3247–3266.

Cai Q, Van der Hagen L, Brysbaert M. 2013. Complementary hemispheric specialization for language production and visuospatial attention. Proc Natl Acad Sci. 110:322–330.

Caspers S, Zilles K, Laird AR, Eickhoff SB. 2010. ALE meta-analysis of action observation and imitation in the human brain. Neuroimage. 50:1148–1167.

Chikazoe J, Jimura K, Asari T. 2009. Functional dissociation in right inferior frontal cortex during performance of go/no-go task. Cereb Cortex. 19:146–152.

Cieslik EC, Zilles K, Caspers S, Roski C, Kellermann TS, Jakobs O, Langer R, Laird AR, Fox PT, Eickhoff SB. 2012. Is there "one" DLPFC in cognitive action control? Evidence for heterogeneity from co-activation-based parcellation. Cereb Cortex. 23:223–229.

Clos M, Amunts K, Laird AR, Fox PT, Eickhoff SB. 2013. Tackling the multifunctional nature of Broca's region meta-analytically: co-activation-based parcellation of area 44. Neuroimage. 83:174–188.

Cole MW, Schneider W. 2007. The cognitive control network: integrated cortical regions with dissociable functions. Neuroimage. 37:343–360.

Corbetta M, Akbudak E, Conturo TE, Snyder AZ, Ollinger JM, Drury HA, Lineweber MR, Petersen SE, Raichle ME, Van Essen DC, et al. 1998. A common network of functional areas for attention and eye movements. Neuron. 21:761–773.

Corbetta M, Shulman GL. 2002. Control of goal-directed and stimulus-driven attention in the brain. Nat Rev Neurosci. 3:201–215.

Crittenden BM, Duncan J. 2014. Task difficulty manipulation reveals multiple demand activity but no frontal lobe hierarchy. Cereb Cortex. 24:532–540.

Curtis CE, D'Esposito M. 2003. Persistent activity in the prefrontal cortex during working memory. Trends Cogn Sci. 7:415–423.

Davare M, Andres M, Cosnard G, Thonnard J-L, Olivier E. 2006. Dissociating the role of ventral and dorsal premotor cortex in precision grasping. J Neurosci. 26:2260–2268.

De Baene W, Albers AM, Brass M. 2012. The what and how components of cognitive control. Neuroimage. 63:203–211.

Dehaene S, Kreszberg M, Changeux JP. 1998. A neuronal model of global workspace in effortful cognitive tasks. Proc Natl Acad Sci. 95:14529–14534.

Derrfuss J, Brass M, Neumann J, von Cramon DY. 2005. Involvement of the inferior frontal junction in cognitive control: meta-analyses of switching and Stroop studies. Hum Brain Mapp. 25:22–34.

Derrfuss J, Brass M, von Cramon DY. 2004. Cognitive control in the posterior frontolateral cortex: evidence from common activations in task coordination, interference control, and working memory. Neuroimage. 23:604–612.

Derrfuss J, Brass M, von Cramon DY, Lohmann G, Amunts K. 2009. Neural activations at the junction of the inferior frontal sulcus and the inferior precentral sulcus: interindividual variability, reliability, and association with sulcal morphology. Hum Brain Mapp. 30:299–311.

Derrfuss J, Vogt VL, Fiebach CJ, von Cramon DY, Tittgemeyer M. 2012. Functional organization of the left inferior precentral sulcus: dissociating the inferior frontal eye field and the inferior frontal junction. Neuroimage. 59:3829–3837.

Desmurget M, Sirigu A. 2009. A parietal-premotor network for movement intention and motor awareness. Trends Cogn Sci. 13:411–419.

Donsenbach NUF, Fair DA, Miezin FM, Cohen AL, Wenger KK, Dosenbach RAT, Fox MD, Snyder AZ, Vincent JL, Raichle ME, et al. 2007. Distinct brain networks for adaptive and stable task control in humans. Proc Natl Acad Sci. 104: 11073–11078.

Dosenbach NUF, Fair DA, Cohen AL, Schlaggar BL, Petersen SE. 2008. A dual-networks architecture of top-down control. Trends Cogn Sci. 12:99–105.

Dosenbach NUF, Visscher KM, Palmer ED, Miezin F, Wenger KK, Kang HC, Burgund ED, Grimes AL, Schlaggar BL, Petersen SE. 2006. A core system for the implementation of task sets. Neuron. 5:799–812.

Duncan J. 2010. The multiple-demand (MD) system of the primate brain: mental programs for intelligent behaviour. Trends Cogn Sci. 14:172–179.

Duncan J. 2013. The structure of cognition: attentional episodes in mind and brain. Neuron. 8:35–50.

Duncan J, Owen AM. 2000. Common regions of the human frontal lobe recruited by diverse cognitive demands. Trends Neurosci. 23:475–483.

Dux PE, Ivanoff J, Asplund CL, Marois R. 2006. Isolation of a central bottleneck of information processing with time-resolved FMRI. Neuron. 52:1109–1120.

Dux PE, Tombu MN, Harrison S, Rogers BP, Tong F, Marois R. 2009. Training improves multitasking performance by increasing the speed of information processing in human prefrontal cortex. Neuron. 63:127–138.

Eickhoff SB, Bzdok D, Laird AR, Kurth F, Fox PT. 2012. Activation likelihood estimation meta-analysis revisited. Neuroimage. 59:2349–2361.

Eickhoff SB, Bzdok D, Laird AR, Roski C, Caspers S, Zilles K, Fox PT. 2011. Co-activation patterns distinguish cortical modules, their connectivity and functional differentiation. Neuroimage. 57:938–949.

Eickhoff SB, Laird AR, Fox PT, Bzdok D, Hensel L. 2014. Functional segregation of the human dorsomedial prefrontal cortex. Cereb Cortex.

Eickhoff SB, Laird AR, Grefkes C, Wang LE, Zilles K, Fox PT. 2009. Coordinate-based activation likelihood estimation meta-analysis of neuroimaging data: a random-effects approach based on empirical estimates of spatial uncertainty. Hum Brain Mapp. 30:2907–2926.

Fedorenko E, Duncan J, Kanwisher N. 2013. Broad domain generality in focal regions of frontal and parietal cortex. Proc Natl Acad Sci. 110:16616–16621.

Fedorenko E, Duncan J, Kanwisher N. 2012. Language-selective and domain-general regions lie side by side within Broca's area. Curr Biol. 22:2059–2062.

Fedorenko E, Hsieh P-J, Nieto-Castañón A, Whitfield-Gabrieli S, Kanwisher N. 2010. New method for fMRI investigations of

language: defining ROIs functionally in individual subjects. J Neurophysiol. 104:1177–1194.
Feredoes E, Heinen K, Weiskopf N, Ruff C, Driver J. 2011. Causal evidence for frontal involvement in memory target maintenance by posterior brain areas during distracter interference of visual working memory. Proc Natl Acad Sci. 108:17510–17515.
Fox PT, Lancaster JL. 2002. Mapping context and content: the BrainMap model. Nat Rev Neurosci. 3:319–321.
Fox PT, Lancaster JL, Laird AR, Eickhoff SBE. 2014. Meta-analysis in human neuroimaging: computational modelling of large-scale databases. Annu Rev Neurosci. 37:409–434.
Friederici AD, Gierhan SME. 2013. The language network. Curr Opin Neurobiol. 23:250–254.
Gordon EM, Laumann TO, Adeyemo B, Huckins JF, Kelley WM, Petersen SE. 2014. Generation and evaluation of a cortical area parcellation from resting-state correltions. Cereb Cortex. doi:10.1093/cercor/bhu239.
Grefkes C, Ritzl A, Zilles K, Fink GR. 2004. Human medial intraparietal cortex subserves visuomotor coordinate transformation. Neuroimage. 23:1494–1506.
Gruber O, Goschke T. 2004. Executive control emerging from dynamic interactions between brain systems mediating language, working memory and attentional processes. Acta Psychol. 115:105–121.
Hagoort P. 2005. On Broca, brain, and binding: a new framework. Trends Cogn Sci. 9:416–423.
Hartigan JA, Wong MA. 1979. A k-means clustering algorithm. J Roy Stat Soc 28:100–108.
Hartstra E, Kühn S, Verguts T, Brass M. 2011. The implementation of verbal instructions: an fMRI study. Hum Brain Mapp. 32:1811–1824.
Jeannerod M, Arbib MA, Rizzolatti G, Sakata H. 1995. Grasping objects: the cortical mechanisms of visuomotor transformation. Trends Neurosci. 18:314–320.
Johansen-Berg H, Behrens TEJ, Robson MD, Drobnjak I, Rushworth MFS, Brady JM, Smith SM, Higham DJ, Matthews PM. 2004. Changes in connectivity profiles define functionally distinct regions in human medial frontal cortex. Proc Natl Acad Sci. 101:13335–13340.
Kahnt T, Chang LJ, Park SQ, Heinzle J, Haynes J-D. 2012. Connectivity-based parcellation of the human orbitofrontal cortex. J Neurosci. 32:6240–6250.
Kelly C, Uddin LQ, Shehzad Z, Margulies DS, Castellanos FX, Milham MP, Petrides M. 2010. Broca's region: linking human brain functional connectivity data and non-human primate tracing anatomy studies. Eur J Neurosci. 32:383–398.
Kim C, Johnson NF, Cilles SE, Gold BT. 2011. Common and distinct mechanisms of cognitive flexibility in prefrontal cortex. J Neurosci. 31:4771–4779.
Koechlin E, Jubault T. 2006. Broca's area and the hierarchical organization of human behavior. Neuron. 50:963–974.
Koechlin E, Ody C, Kouneiher F. 2003. The architecture of cognitive control in the human prefrontal cortex. Science. 302: 1181–1185.
Koechlin E, Summerfield C. 2007. An information theoretical approach to prefrontal executive function. Trends Cogn Sci. 11:229–235.
Kouneiher F, Charron S, Koechlin E. 2009. Motivation and cognitive control in the human prefrontal cortex. Nat Neurosci. 12:939–945.
Kuo BC, Stokes MG, Murray AM, Nobre AC. 2014. Attention biases visual activity in visual short-term memory. J Cogn Neurosci. 26:1377–1389.
Laird AR, Eickhoff SB, Rottschy C, Bzdok D, Ray KL, Fox PT. 2013. Networks of task co-activations. Neuroimage. 80:505–514.
Laird AR, Lancaster JL, Fox PT. 2005. BrainMap: the social evolution of a human brain mapping database. Neuroinformatics. 3:65–78.
Levy BJ, Wagner AD. 2011. Cognitive control in the right ventrolateral prefrontal cortex: reflexive reorienting, motor inhibition, and action updating. Ann N Y Acad Sci 1224:40–62.
MacDonald AW, Cohen JD, Stenger VA, Carter CS. 2000. Dissociating the role of the dorsolateral prefrontal and anterior cingulate cortex in cognitive control. Science. 288:1835–1838.
Mars RB, Jbabdi S, O'Reilly JX, Croxson PL, Olivier E, Noonan MP, Bergmann C, Mitchell AS, Baxter MG, Behrens TE, et al. 2011. Diffusion-weighted imaging tractography-based parcellation of the human parietal cortex and comparison with human and macaque resting-state functional connectivity. J Neurosci. 31:4087–4100.
Meila M. 2007. Comparing clusterings—an information based distance. J Multivar Anal. 98:873–895.
Mesulam MM. 1981. A cortical network for directed attention and unilateral neglect. Ann Neurol. 10:309–325.
Muhle-Karbe PS, Andres M, Brass M. 2014. Transcranial magnetic stimulation dissociates prefrontal and parietal contributions to task preparation. J Neurosci. 34:12481–12489.
Muhle-Karbe PS, De Baene W, Brass M. 2014. Do tasks matter in task switching? Dissociating domain-general from context-specific brain activity. Neuroimage. 99:332–341.
Nee DE, Brown JW. 2012. Rostral-caudal gradients of abstraction revealed by multi-variate pattern analysis of working memory. Neuroimage. 63:1285–1294.
Nee DE, Brown JW, Askren MK, Berman MG, Demiralp E, Krawitz A, Jonides J. 2013. A meta-analysis of executive components of working memory. Cereb Cortex. 23:264–282.
Nee DE, Brown JW. 2013. Dissociable frontal-striatal and frontal-parietal networks involved in updating hierarchical contexts in working memory. Cereb Cortex. 23:2146–2158.
Nelson SM, Cohen AL, Power DD, Wig GS, Miezin FM, Wheeler ME, Wheeler ME, Velanova K, DOnaldson DI, Phillips JS, et al. 2010. A parcellation scheme for human left lateral parietal cortex. Neuron. 67:156–170.
Neubert F-X, Mars RB, Thomas AG, Sallet J, Rushworth MFS. 2014. Comparison of human ventral frontal cortex areas for cognitive control and language with areas in monkey frontal cortex. Neuron. 81:700–713.
Neumann J, Lohmann G, Derrfuss J, von Cramon DY. 2005. The meta-analysis of functional imaging data using replicator dynamics. Hum Brain Mapp. 25:165–173.
Nichols T, Brett M, Andersson J, Wager T, Poline JB. 2005. Valid conjunction inference with the minimum statistic. Neuroimage. 25:653–660.
Niendam TA, Laird AR, Ray KL, Dean YM, Glahn DC, Carter CS. 2012. Meta-anlytic evidence for a superordinate cognitive control network subserving diverse executive functions. Cogn Affect Behav Neurosci. 12:241–268.
Passingham RE, Stephan KE, Kötter R. 2002. The anatomical basis of functional localization in the cortex. Nat Rev Neurosci. 3:606–616.
Paus T. 1996. Location and function of the human frontal eye-field: a selective review. Neuropsychologia, 34:475–483.
Petrides M. 2000. The role of the mid-dorsolateral prefrontal cortex in working memory. Exp Brain Res. 133:44–54.
Poldrack RA. 2006. Can cognitive processes be inferred from neuroimaging data? Trends Cogn Sci 10:59–63.
Poldrack RA. 2011. Inferring mental states from neuroimaging data: from reverse inference to large-scale decoding. Neuron. 72:692–697.

Power JD, Cohen AL, Nelson SM, Wig GS, Barnes KA, Church JA, Vogel AC, Laumann TO, Miezin FM, Schlaggar BL, et al. 2011. Functional network organization of the human brain. Neuron. 72:665–678.

Reynolds JR, O'Reily DD, Cohen JD, Braver TS. 2012. The function and organization of the lateral prefrontal cortex: a test of competing hypotheses. PLoS ONE. 7:e30284.

Rizzolatti G, Fogassi L, Gallese V. 2002. Motor and cognitive functions of the ventral premotor cortex. Curr Opin Neurobiol. 12:149–154.

Rottschy C, Langer R, Dogan I, Reetz K, Laird AR, Schulz JB, Fox PT, Eickhoff SBE. 2012. Modelling neural correlates of working memory: a coordinate-based meta-analysis. Neuroimage. 60:830–846.

Ruge H, Wolfensteller U. 2010. Rapid formation of pragmatic rule representations in the human brain during instruction-based learning. Cereb Cortex. 20:1656–1667.

Rushworth MFS, Ellison A, Walsh V. 2001. Complementary localization and lateralization of orienting and motor attention. Nat Neurosci. 4:656–661.

Rushworth MFS, Johansen-Berg H, Göbel S, Devlin J. 2003. The left parietal and premotor cortices: motor attention and selection. Neuroimage. 20:89–100.

Rushworth MFS, Krams M, Passingham RE. 2001. The attentional role of the left parietal cortex: the distinct lateralization and localization of motor attention in the human brain. J Cogn Neurosci. 13:698–710.

Sallet J, Mars RB, Noonan MP, Neubert F-X, Jbabdi S, O'Reilly JX, Filippini N, Thomas AG, Rushworth MFS. 2013. The organization of dorsal frontal cortex in humans and macaques. J Neurosci. 33:2255–12274.

Smith SM, Fox PT, Miller KL, Glahn DC, Fox PM, Mackay CE, Filippini N, Watkins KE, Toro R, Laird AR, et al. 2009. Correspondence of the brain's functional architecture during activation and rest. Proc Acad Natl Sci. 106:13040–13045.

Sneve MH, Magnussen S, Alnæs D, Endestad T, Esposito MD. 2013. Top–down modulation from inferior frontal junction to FEFs and intraparietal sulcus during short-term memory for visual features. J Cogn Neurosci. 25:1944–1956.

Stephan KE, Marshall JC, Friston KJ, Rowe JB, Ritzl A, Zilles K, Fink GR. 2003. Lateralized cognitive processes and lateralized task control in the human brain. Science. 301:384–386.

Todd JJ, Han SW, Harrison S, Marois R. 2011. The neural correlates of visual working memory encoding: a time-resolved fMRI study. Neuropsychologia. 49:1527–1536.

Tombu MN, Asplund CL, Dux PE, Godwin D, Martin JW, Marois R. 2011. A unified attentional bottleneck in the human brain. Proc Natl Acad Sci. 108:13426–13431.

Turkeltaub PE, Eden GF, Jones KM, Zeffiro TA. 2002. Meta-analysis of the functional neuroanatomy of single-word reading: method and validation. Neuroimage. 16:765–780.

Turkeltaub PE, Eickhoff SB, Laird AR, Fox M, Wiener M, Fox P. 2012. Minimizing within-experiment and within-group effects in activation likelihood estimation meta-analyses. Hum Brain Mapp. 33:1–13.

Verbruggen F, Aron AR, Stevens MA, Chambers CD. 2010. Theta burst stimulation dissociates attention and action updating in human inferior frontal cortex. Proc Natl Acad Sci. 107: 13966–13971.

Vigneau M, Beaucousin V, Hervé PY, Duffau H, Crivello F, Houdé O, Mazoyer B, Tzourio-Mazoyer N. 2006. Meta-analyzing left hemisphere language areas: phonology, semantics, and sentence processing. Neuroimage. 30:1414–1432.

Wang J, Yang Y, Fan L, Xu J, Li C, Liu Y, Fox PT, Eickhoff SB, Yu C, Jiang T. forthcoming. Convergent functional architecture of the superior parietal lobule unraveled with multimodal neuroimaging approaches. Hum Brain Mapp.

Wig GS, Laumann TO, Cohen AL, Power JD, Nelson SM, Glasser MF, Miezin FM, Snyder AZ, Schlaggar BL, Petersen SE. 2013. Parcellating an individual subject's cortical and subcortical brain structures using snowball sampling of resting-state correlations. Cereb Cortex. 24:2036–2054.

Wig GS, Laumann TO, Petersen SE. 2014. An approach for parcellating human cortical areas using resting-state correlations. Neuoimage 93:276–291.

Wise SP. 1985. The primate premotor cortex: past, present, and preparatory. Annu Rev Neurosci. 8:1–19.

Wise SP, Boussaoud D, Johnson PB, Caminiti R. 1997. Premotor and parietal cortex: corticocortical connectivity and combinatorial computations. Annu Rev Neurosci. 20:25–42.

Woolgar A, Thompson R, Hampshire A, Duncan J. 2011. Adaptive coding of task-relevant information in human frontoparietal cortex. J Neurosci. 31:14592–14599.

Yarkoni T, Poldrack RA, Nichols TE, Van Essen DC, Wager TD. 2011. Large-scale automated synthesis of human functional neuroimaging data. Nat Methods. 8:665–670.

Yeo BTT, Krienen FM, Sepulcre J, Sabuncu MR, Lashkari D, Hollinshead M, Roffman JL, Smoller JW, Zöllei L, Polimeni JR, et al. 2011. The organization of the human cerebral cortex estimated by intrinsic functional connectivity. J Neurophysiol. 106:1125–1165.

Zanto TP, Rubens MT, Bollinger J, Gazzaley A. 2010. Top-down modulation of visual feature processing: the role of the inferior frontal junction. Neuroimage. 53:736–745.

Zanto TP, Rubens MT, Thangavel A, Gazzaley A. 2011. Causal role of the prefrontal cortex in top-down modulation of visual processing and working memory. Nat Neurosci. 14: 656–661.

Zysset S, Müller K, Lohmann G, von Cramon DY. 2001. Color-word matching Stroop task: separating interference and response conflict. Neuroimage. 13:29–36.